Optimal Stiffness Tuning for a Lower Body Exoskeleton with Spring-Supported Passive Joints

Mehmet C. Yildirim, Polat Sendur, Ahmed Fahmy Soliman, and Barkan Ugurlu

***Abstract*— This paper presents a framework to optimally tune the stiffness values of spring-supported passive joints that are included in lower body exoskeletons. First, a dynamic model of a combined human-exoskeleton system was created in MSC.ADAMS software. Second, a gradient-descent based algorithm was used to find the optimum value to minimize the ZMP for a range of ankle stiffness values. In order to corroborate the proposed method, simulation experiments were conducted by considering three cases in which different body mass and heights were assigned to the combined human-exoskeleton system. The simulation results indicate that the proposed methodology is effective in order to find the optimum ankle stiffness for the combined human-exoskeleton systems, resulting in reductions in ZMP variations and therefore increasing the balancing ability. As a consequence, it may be possible to reduce the number of active joints in exoskeletons that aim crutch-free 3-D walking motion support.**

I. Introduction

Powered lower body exoskeletons are proven to be useful systems to help paraplegics gain walking ability with the aid of robots [1]. The state-of-the-art lower body exoskeletons usually have two active degrees of freedom (DoF) at the knee and hip joints, along the flexion/extension (F/E) axis [2]–[9]. Such a kinematic configuration can move the user's leg forward; however, it does not suffice for balancing or even standing still. Therefore, the user needs to involve her/his upper body via crutches to maintain static balance.

In order to achieve self-balancing during robot-aided walking, it is required to increase the number of active DoFs. For example, an active ankle joint along the flexion/dorsiflexion (D/F) axis is necessary [10], [11]. Moreover, the 3-D walking motion dictates that the Human Body Center of Mass (BCM) must be laterally swayed; therefore, a hip adduction/abduction (A/A) joint should be added as well [12], [13]. Following this strategy, a crutch-free walking support could be provided by the fully-actuated exoskeletons, which also include an active ankle I/E (roll axis) joint [14], [15].

Increasing the number of active joints evidently helps the cause of self-sustained walking with the expanse of increased overall weight. In particular, the high torque output requirement enforces engineers to make use of large motors with gear boxes, causing these systems to be relatively bulky. This may reduce the patient acceptance and may cause comparatively slow walking performance.

The authors are with the Faculty of Engineering, Department of Mechanical Engineering, Ozyegin University, 34794 Istanbul, Turkey. {polat.sendur,barkan.ugurlu}@ozyegin.edu.tr, {mehmet.yildirim,fahmy.ahmed}@ozu.edu.tr

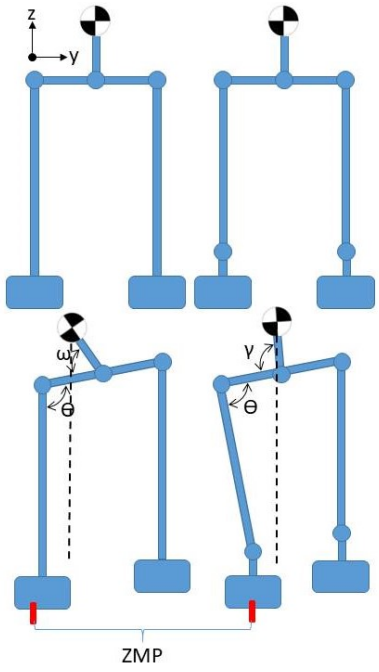

Fig. 1. The changes in ZMP and upper body torso angle with the addition of an ankle I/E joint compared to a fixed ankle joint. For the case of no passive ankle I/E joint, the hip A/A rotation must be large to provide the desired CoM position. In contrast, for the case with passive ankle I/E joint, the hip A/A joint rotates less as the ankle I/E joints also contributes. As a result, both torso angle and ZMP can be well contained.

In [16], it is shown that the the minimum requirement to realize 3-D walking motion is by equipping each leg with 4 active joints, namely, a 2-DoF hip joint along the F/E and A/A axes, a 1-DoF knee joint along the F/E axis and a 1-DoF ankle joint along the F/E axis. While this joint configuration provides the means for a kinematically feasible walking motion, the upper body orientation along the lateral axis is relatively large when compared to a healthy person's upper body motion; see Fig. 1. This leads to aggressive changes in the Zero Moment Point (ZMP), an important balance criterion to assess the consistency of walking motion [17].

One possible solution to the aforementioned problems is to make use of spring-supported passive joints [18], [19]. Since the robot-aided paraplegia walking support includes predetermined trajectories, one may exploit the passivity property via offline simulations to come up with an optimum stiffness value that provides relatively more efficient locomotion. An exemplary work that exploits the spring potential was provided by Tsagarakis et al., where the stiffness values were

optimized for maximum energy efficiency of a humanoid with series elastic actuators (SEA) [20]. A similar approach was executed by exploiting the base resonance frequency to generate hopping locomotion [21]. Springs were also coupled with clutch mechanisms to provide power assistance [22].

Despite the fact that the efficacy of passivity were well demonstrated in the legged locomotion research, only a handful of exoskeleton systems are equipped with springs [19]. Considering the fact that the recent trend in exoskeleton hardware development suggests increasing the number of active joint for greater motion flexibility, we argue that spring-supported passive joints may provide the same effect while reducing the power consumption, weight and size. The stiffness tuning on the other hand has not been fully addressed and this paper aims to contribute towards this direction.

In the light of the facts discussed above, this paper presents a framework to optimally tune the stiffness values of spring-supported passive joints of exoskeletons. In particular, we focused on the 4-DoF-per-leg model provided in [16], and added a spring-supported passive ankle joint along the inversion/eversion (I/E) axis. Using MSC.ADAMS and MATLAB co-simulation, an optimization routine was devised to explore the optimal stiffness value that minimizes ZMP to improve active balancing. For a given target sway trajectory, we showed the variance in optimal passive joint stiffness values with respect to overall mass and height of the combined human-exoskeleton system in question.

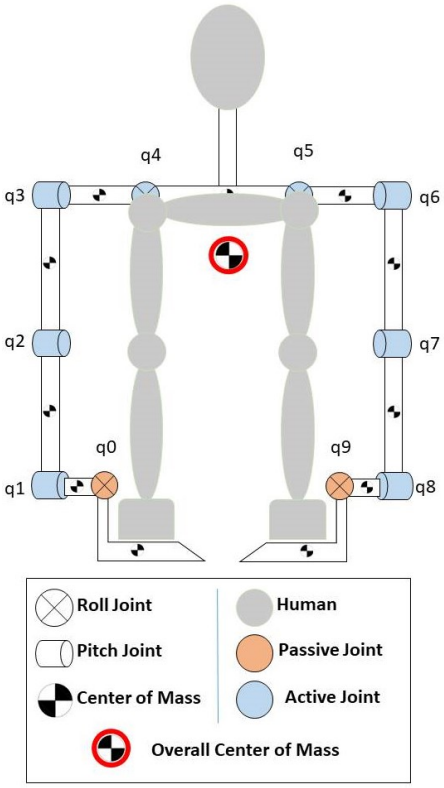

Fig. 2. CoM positions of the exoskeleton joints, joint configuration of the exoskeleton and the overall CoM position of the combined exoskeleton/human model

II. Method

A. Compliant Body Modeling

An MSC.ADAMS (version 2016) model was developed to simulate dynamics of the system, where the equivalent parameters representing the combined human and exoskeleton system such as mass, inertia were used; see Fig. 3. The input data for exoskeleton parameters were obtained from the modular design of Bartenbach et al. [18], in wihch CAD data for an exoskeleton with 8 active joints was shared publicly. The actuator specifications were obtained from [23]. Whereas, human parameters were obtained from [24] and [25]. The following modeling approach was taken into account to model distance between Hip A/A and Hip E/F joints: The femur head was accepted as the Hip A/A joint's rotation axis and the Hip E/F joint to Hip A/A joint length value was adjusted in accordance with the distance between fovea capitis and greater trochater of the femur; see Fig. 2. Additionally, in accordance with Leardini et al.'s data [26], maximum deflection of the ankle's passive joint was limited to 20°.

As depicted in Fig. 4, spring torques from the passive joints of the system, were calculated in MATLAB software. MSC.ADAMS model was exported as a transfer function to MATLAB/Simulink using ADAMS.Controls plug-in, where the inputs to the model were active joint angles and the torque values created by the passive springs on the ankle's I/E joints, while the outputs were the angles and the angular velocities of the ankle's I/E joints and the Reaction Force (Fz) and Pitch Moment (Mx). For every time step, the torques were calculated from Simulink and sent to MSC.ADAMS. Similarly, MSC.ADAMS model calculated the angles of the joints and sent the results to Simulink. MSC.ADAMS macro codes were developed in order to facilitate the development and adjustment to humans of different sizes. In all cases, the mass of the exoskeleton was considered as the same. The MSC.ADAMS model was developed as capable to calculate the equivalent mass and inertia for the combined human-exoskeleton system for different subjects based on given total body weight and the body height with respect to average human body ratios given in [24], [25]. CAD drawings of the components were not associated with the rigid bodies in the model in order to reduced the computational complexity of the simulation. As previously mentioned, inertia and mass properties were calculated separately, then were considered as the inputs to the MSC.ADAMS's model. Rigid body models were represented with their mass and mass moment of inertiae located at their respective CoM. Mass moment of inertia values were defined with respect to the body moving coordinate system at the CoM. The MSC.ADAMS model of the system is shown in Fig. 3. The model has 25 parts, 10 revolute joints, 14 fixed joints and 8 general motion constraints to prescribe the kinematics of the joints resulting in a 8-DoF system. The overall mass of the model is 138 kg (100 kg human and 38 kg exoskeleton) and CoM of the model is shown in Fig. 2, MSC.ADAMS-MATLAB/Simulink

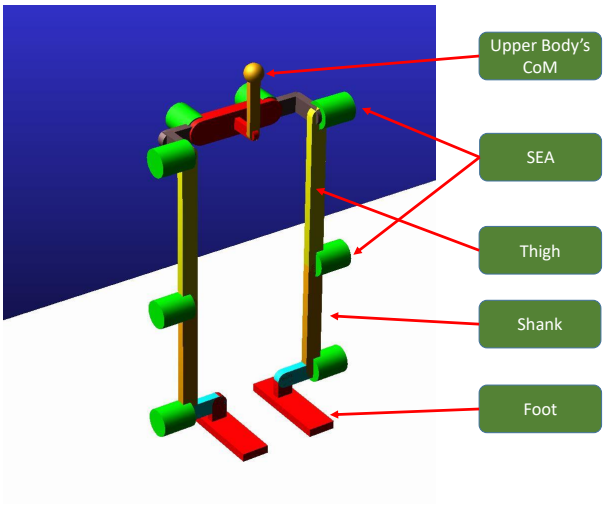

Fig. 3. Combined Human-Exoskeleton Model on the MSC.ADAMS environment. Upper body's CoM is a lump model of the human's upper body with both mass and inertia values. Furthermore passive joints are not visually represented in this model.

co-simulation environment is shown in Fig. 4.

TABLE I

STRUCTURE AND THE STIFFNESS PARAMETERS OF THE ANALYZED MODEL

			Structure	Torque Capacity	Stiffness
1	Ankle	Inversion & Eversion	Passive	—	To Be Determined
2	Ankle	Flexion & Dorsiflexion	Active	95 (Nm)	5220 (Nm/rad)
3	Knee	Extension & Flexion	Active	95 (Nm)	5220 (Nm/rad)
4	Hip	Extension & Flexion	Active	95 (Nm)	5220 (Nm/rad)
5	Hip	Adduction & Abduction	Active	95 (Nm)	5220 (Nm/rad)

The impact function of MSC.ADAMS was used in order to model the interaction between the foot and floor. The foot was modeled using a rectangular box shape. Contrary to the parametric model of the dynamic model, foot sizes were adjusted with respect to the tallest human case. Constant foot size for all three cases was used as this is a common modeling approach in the literature [13]. The ground was represented by a flat rigid surface. Depending on the level of penetration between the geometries of foot and floor, the contact force was calculated as follows,

$$F = kx^e - \dot{x}c_{max}u(x), \tag{1}$$

where k is the stiffness representing the contact stiffness, x is the penetration between the geometries of foot and floor, c_{max} is the maximum damping coefficient and d is the penetration at which the maximum damping is applied, $u(x)$ is a step function. The parameter, force exponent e, defines the force deformation characteristics. Values of $e > 1$ is used to represent increasing stiffness with the penetration depth, while $e < 1$ is used where the contact force decreases with penetration. The value of $e = 1$ represents a linear spring. In the model, the contact parameters are chosen as: $k = 1.0E + 006\ N/m$, $e = 1$, $c_{max} = 1.0E + 004\ Ns/m$, $d = 0.1\ mm$.

B. Stiffness Optimization

An optimization study was performed to find the optimum value of the stiffness of the ankle. The objective function was chosen as to minimize the integral of the absolute value of ZMP. An additional parameter was added to the objective function in order to penalize conditions when there is no contact between the foot and the ground. The objective function is shown as follows.

$$f = min(\int_{t=0}^{T}(|ZMP| + P)dt) \tag{2}$$

where ZMP is the momentary ZMP value of the system and the P is the penalty value. To set the penalty value, the resultant ZMP values were sampled with different stiffness values K, and the maximum momentary ZMP value was chosen as the current penalty value.

$$1000 < K < 5000 \tag{3}$$

The lower and upper bounds were found by performing several simulations prior to optimization runs to make sure that it covers the range of the ankle. More specifically, a variety of different K values were simulated. After a careful investigation of the simulation results by trying random K values, it is concluded that with lower K values the human/exoskeleton model tips over laterally towards the sway direction. On the contrary, for higher K values, the system bounces back and tips toward the opposite direction of the motion.

In (3), K is the stiffness of the ankle. If the optimization converges to either lower or to upper values, then the boundaries were defined to cover a wider range and the optimization was re-run.

Simulink's Response Optimization toolbox was used for the optimization study. MSC.ADAMS was used as the solver. Simulink/ADAMS co-simulation with interactive option was performed for the numerical integration and calculation of the objective function. Sequential Quadratic Programming (SQP), a gradient descent based algorithm, was selected as the optimization algorithm. Tolerances on the constraints and objective function were set to 0.001. Maximum iteration number was set to 100. During the optimization solution phase, the objective function was monitored for each iteration to make sure that the optimization converges.

C. Sway Trajectory Generation

Reference joint angle trajectory were generated via a prioritization-based inverse kinematic algorithm that considered only the 8 active joints [16]. As an example, hip A/A and BCM trajectory references are displayed in Fig. 5.

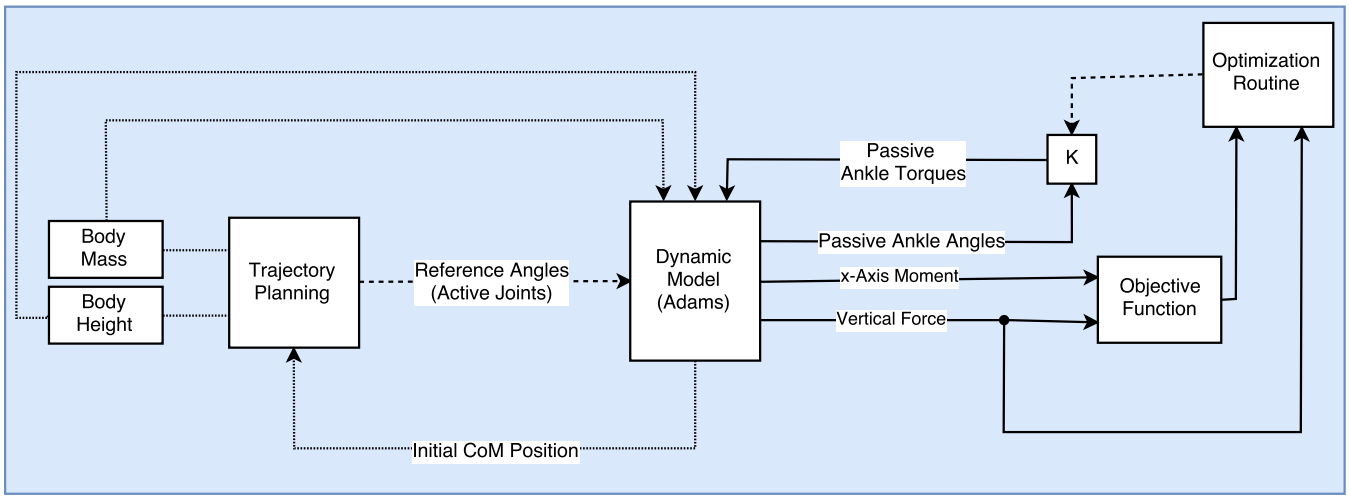

Fig. 4. Work Flow of the suggested optimization model

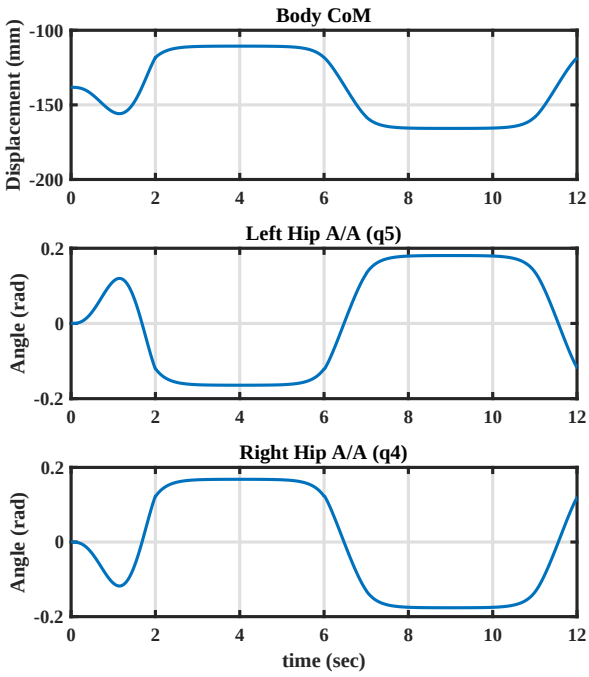

Fig. 5. Hip A/A angles and BCM position of the generated sway trajectory (top) BCM position with respect to left foot (middle) Left Hip (bottom) Right Hip

TABLE II

DETAILED PARAMETER INFORMATION OF RANDOMLY CHOSEN CASES

Cases		1	2	3
Body Height	cm	190	175	160
Body Weight	kg	100	80	65
Total Weight	kg	138	118	103
CoM Height	cm	91.1	86.2	82.3

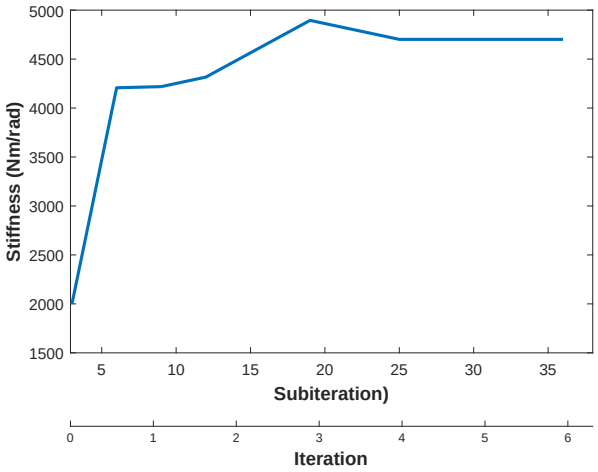

Fig. 6. Stiffness vs. optimization iteration (subiteration) for initial case

Since the two pre-determined passive joints are locked, the generated Inverse Kinematics (IK) solution uses only 8-DOF to control body center of mass (BCM). The MSC.ADAMS-MATLAB co-simulation model takes into account the flexibility in the ankle joint, which was considered as perfectly rigid in the reference joint angle trajectory generation phase.

The proposed methodology was applied to the models with different body weight and height as part of various case studies. Three case studies are summarized in Table II.

III. RESULTS

The optimization is first applied to Case 1. For the initial value of the stiffness K = 2000 Nm/rad was chosen. The optimization converged to an optimum value of $Kopt$ = 4701 Nm/rad after 6 iterations and 36 subiterations. The convergence of the stiffness as a function of iterations and subiterations is shown in Fig. 6.

In Fig. 7, the response of the passive joints with different stiffness values are given with the optimized stiffness value of 4701 Nm/rad for Case 1. Initial value of K = 5500 Nm/rad, a considerably high stiffness value, it is observed

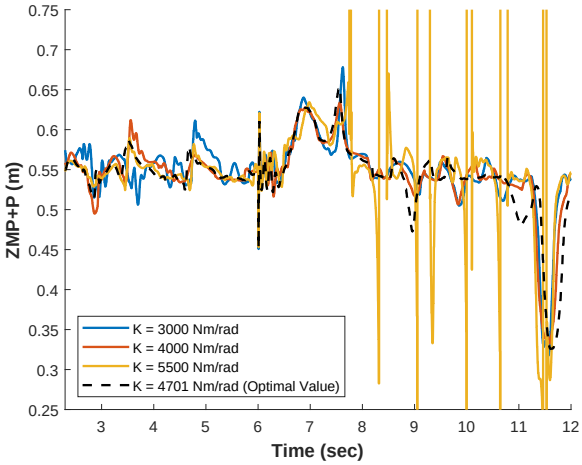

Fig. 7. Comparison of objective function results with different stiffness (K) values

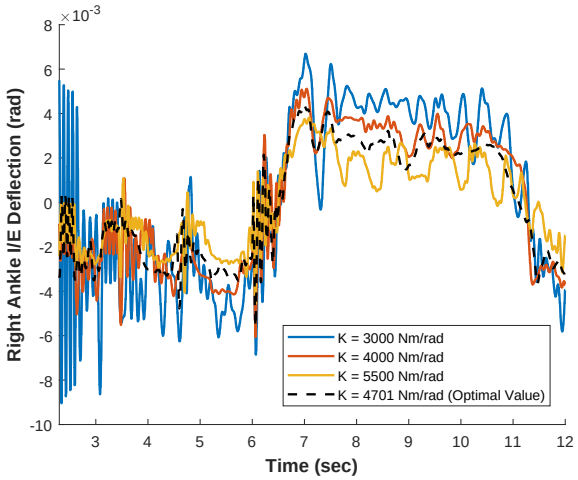

Fig. 8. Comparison of Right Ankle I/E deflection values with different stiffness values

that the model's foot lose its contact from the ground. Therefore, a penalization is added to the objective function in accordance with (2). This could be seen from the step increases on the time response of the system shown in Fig. 7. On the other hand, the objective function values which are lower than the general trend of the same graph are the result of the impact when the foot hits the ground. The impact to ground results in higher forces on the foot, the moment with respect to x-axis (roll) is constant. For relatively lower K values (3000Nm/rad and 4000 Nm/rad) even the ZMP values get closer to an almost constant range; the variation of the response was reduce as K value reaches to the optimum value of 4701 Nm/rad.

The algorithm was then applied to the other two case studies. Similar convergence results in terms of the number of the iterations as the first case study were obtained, and therefore the results were not plotted for the sake of conciseness. The optimum stiffness values for three case studies mentioned in Table II are 4701 Nm/rad, 2134 Nm/rad, and 697 Nm/rad for Case 1, Case 2 and Case 3, respectively. In Fig. 8 the angular deflection of the ankle's I/E joints with different stiffness values are plotted with respect to time.

IV. Discussion

In this pilot study, a lateral swaying motion was considered since the passive joints are most effective in the plane of swaying motion. The forces created by the active hip joints during sway motion can be balanced with only the ankle I/E joints. For more complex motion like walking, loads on the passive ankle joints can be result from a much more complicated dynamics interactions. On the other hand, the motion of the passive ankles is more dominant during lateral swaying motion than walking due to support by both feet compared to one foot raised during walking [27]. Losing the balance of the system under swaying is of great concern, which is only possible when the active joints can not track the desired motion under external disturbances. One possible example of losing the balance is due to low ankle stiffness where the system may fall sideways. It is important to observe the higher oscillation amplitudes corresponding to lower and higher stiffness values compared to the much lower oscillations for the optimal stiffness value. The results suggest that the stiffness should be carefully engineered to minimize oscillations during 3D walking and similar dynamic movements.

The simulation results showed that the optimum K value change with respect to body mass and body height of the human. Further simulations are needed in order to quantify the relation between the mass/height of the system. Since these parameters are affected by more than 28 different physical quantatity of the human body and the exoskeleton, this study was acknowledged as a future work.

V. Conclusion

In this study, a passive joint stiffness optimization was performed to find the optimum stiffness value, which can adequately provide the required hip motion and still support the overall weight of the system. The sway motion simulation results from the three case studies considered indicate that optimization depends on many factors such as the CoM of the human/exoskeleton system and the weight of the system. Since an adjustable exoskeleton is used for the model, mass and inertia of the exoskeleton become more dominant for a short user. In addition, the effect of other parameters such as single limb lengths, torso's mass ratio, etc. can be investigated. In this study, a generic human body mass and inertia distribution based on healthy human population was used. However, body mass distribution of a paraplegic patient can be quite different than that of healthy a human. The analysis and the optimization of the system with body mass, inertia, and height values of paraplegic patients via experimental investigations are acknowledged as future work.

ACKNOWLEDGMENT

This work is supported by the Scientific and Technological Research Council of Turkey (TÜBİTAK), with the project 215E138. M.C. Yildirim acknowledges COST Actions Inclusiveness Target Countries (ITC) Conference Travel Support Grant CA16116. The authors thank A.T. Kansizoglu and B. Balci for their supports.

REFERENCES

[1] A. J. Young and D. P. Ferris "State of the Art and Future Directions for Lower Limb Robotic Exoskeletons", IEEE Transactions on Neural Systems and Rehabilitation Engineering, vol. 25, no. 2, pp. 171-182.

[2] B. Ugurlu, H. Oshima, and T. Narikiyo "Lower Body Exoskeleton-Supported Compliant Bipedal Walking for Paraplegics: How to Reduce Upper Body Effort?", in proceedings of IEEE International Conference on Robotics and Automation, Hong Kong, China 2014, pp. 1354-1360.

[3] L. Benner "Exploring the Psychosocial Impact of Ekso Bionics Technology" Archives of Physical Medicine and Rehabilitation, vol. 97, no. 10, pp. 113.

[4] S. O. Schrade, K. Dätwyler, M. Stucheli, K. Studer, D. A. Turk, M. Meboldt, R. Gassert, and O. Lambercy "Development of VariLeg, an exoskeleton with variable stiffness actuation: first results and user evaluation from the CYBATHLON" Journal of NeuroEngineering and Rehabilitation, vol. 15, no. 1, 2016, pp. 1-18.

[5] K. Strausser, T. Swift, A. Zoss, H. Kazerooni and B. Bennett, "Mobile Exoskeleton for Spinal Cord Injury: Development and Testing", in ASME 2011 Dynamic Systems and Control Conference and Bath/ASME Symposium on Fluid Power and Motion Control, Virginia, USA, 2018, pp. 419-425.

[6] "Austin — Berkeley Robotics and Human Engineering Laboratory," Bleex.me.berkeley.edu, 2018. [Online]. Available: http://bleex.me.berkeley.edu/research/exoskeleton/medical-exoskeleton/. [Accessed: 13- Feb- 2018].

[7] S.V. Kotov, V.Y. Lijdvoy, A.B. Sekirin, K.A. Petrushanskaya, and E.V. Pismennaya "The efficacy of the exoskeleton ExoAtlet to restore walking in patients with multiple sclerosis." Zhurnal nevrologii i psikhiatrii imeni SS Korsakova, vol. 117 no. 10, 2017 pp. 41-47.

[8] M. Talaty, A. Esquenazi, and J. E. Briceno, "Differentiating ability in users of the ReWalk powered exoskeleton: An analysis of walking kinematics," in Proc. IEEE International Conference on Rehabilitation Robotics, Seattle, WA, USA, 2013, pp. 1-5.

[9] R. J. Farris. "Design of a Powered Lower-Limb Exoskeleton and Control for Gait Assistance in Paraplegics" Doctor of Philosophy, Graduate School of Vanderbilt University, Nasville, Tennessee, USA, 2012.

[10] "HANK Exoskeleton design - Gogoa", Gogoa, 2018. [Online]. Available: http://gogoa.eu/technology/hank-exoskeleton-design/. [Accessed: 13- Feb- 2018].

[11] B. Ugurlu, C. Doppmann, M. Hamaya, P. Forni, T. Teramae, T. Noda, and J. Morimoto Variable Ankle Stiffness Improves Balance Control: Experiments on a Bipedal Exoskeleton", IEEE/ASME Transactions on Mechatronics, vol. 21, no. 1, pp.79-87, 2016.

[12] T. Vouga, R. Baud, J. Fasola, M. Bouri, and H. Bleuler "TWIICE – A Lightweight Lower-limb Exoskeleton for Complete Paraplegics" in proc. IEEE International Conference on Rehabilitation Robotics, London, UK, 2017, pp. 1639-1645

[13] S. Wang, L. Wang, C. Meijneke, E. van Asseldonk, T. Hoellinger, G. Cheron, Y. Ivanenko, V. La Scaleia, F. Sylos-Labini, M. Molinari, F. Tamburella, I. Pisotta, F. Thorsteinsson, M. Ilzkovitz, J. Gancet, Y. Nevatia, R. Hauffe, F. Zanow, and H. van der Kooij "Design and Control of the MINDWALKER Exoskeleton", IEEE Transactions on Neural Systems and Rehabilitation Engineering, vol. 23, no. 2, 2015, pp. 277-286.

[14] G. Barbareschi, R. Richards, M. Thornton, T. Carlson, C. Holloway "Statically vs dynamically balanced gait: analysis of a robotic exoskeleton compared with a human" in Proc. Int. Conf. of the IEEE Engineering in Medicine and Biology Society , Milan, Italy, 2015, pp. 6728-6731.

[15] A. Agrawal, O. Harib, A. Hereid, S. Finet, M. Masselin, L. Praly, A. D. Ames, K. Sreenath, and J. W. Grizzle, "First Steps Towards Translating HZD Control of Bipedal Robots to Decentralized Control of Exoskeletons" in IEEE Access, vol. 5, 2017, pp. 9919-9934.

[16] A. F. Soliman, B. Ugurlu, "A Task Prioritization-based Inverse Kinematics Algorithm for an Underactuated Exoskeleton", Turkish Conference on Robotics Science, 2018.

[17] M. Vukobratovic, B. Borovac, "Zero Moment Point - Thirty Five Years of its Life", Int. Journal of Humanoid Robots, vol. 1, no. 1, 2004, pp. 157-173.

[18] V. Bartenbach, M. Gort, and R. Riener, "Concept and design of a modular lower limb exoskeleton." in Proc. IEEE International Conference on Biomedical Robotics and Biomechatronics, 2016, pp.649-654.

[19] J. E. Pratt, B. T. Krupp, C. J. Morse, and S. H. Collins "The RoboKnee: An Exoskeleton for Enhancing Strength and Endurance During Walking " in Proc. Int. Conf. of the IEEE International Conference on Robotics and Automation , New Orleans, USA, 2004, pp. 2430-2435.

[20] N. G. Tsagarakis, S. Morfey, G. Medrano-Cerda, Z. Li, and D. G. Caldwell, "Compliant humanoid Coman: Optimal joint stiffness tuning for modal frequency control," in proc. of the IEEE Int. Conf. on Robotics and Automation, Karlsruhe, Germany, 2013, pp. 673-678.

[21] B. Ugurlu, J. A. Saglia, N. G. Tsagarakis, S. Morfey, and D. G. Caldwell "Bipedal hopping pattern generation for passively compliant humanoids: Exploiting the resonance", IEEE Transactions on Industrial Electronics, vol. 61, no. 10, pp. 5431-5443, 2014.

[22] J. Zhang, P. Fiers, K. A. Witte, R. W. Jackson, K. L. Poggensee, C. G. Atkeson, and S. H. Collins, "Human-in-the-loop optimization of exoskeleton assistance during walking" in Science, vol. 356, no. 6344, 2017, pp. 1280-1284.

[23] M. C. Yildirim, P. Sendur, O. Bilgin, B. Gulek, G. G. Yapici, and B. Ugurlu, "An integrated design approach for a series elastic actuator: Stiffness formulation, fatigue analysis, thermal management" in Proc. of the IEEE-RAS International Conference on Humanoid Robots , Birmingham, UK, 2017, pp. 384-389.

[24] P. De Leva, "Adjustments to Zatsiorsky-Seluyanov's segment inertia parameters." in Journal of Biomechanics, vol. 29, no. 9, 1223-1230, 1996.

[25] R. Dumas, L. Cheze, and J.P. Verriest "Adjustments to McConville et al. and Young et al. body segment inertial parameters." in Journal of Biomechanics, vol. 40, no. 3, 543-553, 2007.

[26] A. Leardini, J. J. O'Connor, F. Catani, S. Giannini, "Kinematics of the human ankle complex in passive flexion; a single degree of freedom system", Journal of Biomechanics, vol. 32, no. 2, 1999, pp. 111-118.

[27] D. A. Winter, A. E. Patla, S. Rietdyk, and M. G. Ishac, "Ankle muscle stiffness in the control of balance during quiet standing." Journal of Neurophysiology, vol. 85, no. 6, 2630-2633, 2001.